preprint version of: J. Phys. Chem. Sol. 106, 52-57 (2017), published version © 2017 Elsevier Ltd.
link to published version: http://dx.doi.org/10.1016/j.jpcs.2017.02.016

NMR Study of Vacancy and Structure-Induced Changes in $Cu_{2-x}Te$

Ali A. Sirusi[a], Alexander Page[b], Ctirad Uher[b], Joseph H. Ross, Jr.[a,c,*]

[a] *Department of Physics and Astronomy, Texas A&M University, College Station, Texas 77843, USA*
[b] *Department of Physics, University of Michigan, Ann Arbor, MI 48109, USA*
[c] *Department of Materials Science and Engineering, Texas A&M University, College Station, Texas 77843, USA*

Abstract

We report Cu and Te NMR measurements on $Cu_{2-x}Te$ with x between 0.13 and 0.22. Aided by powder x-ray analysis and computed NMR quadrupole shifts, a structure change near $x = 0.20$ was found consistent with structures reported by Baranova, with best fits to the β-I structure for $x = 0.22$ and β-III for smaller x. NMR T_1 and Hall effect results demonstrate p-type electronic behavior with filling of simple hole pockets induced by increased numbers of vacancies for both phases. Furthermore the Cu and Te chemical shifts are large and negative, as observed in topologically inverted semiconductors, with a splitting into two distinct local environments for both Cu and Te sites in the $x = 0.22$ structure. Cu T_1 results show a rapid decrease of the energy barrier for initiation of Cu ion hopping to 0.12 eV for $x = 0.22$, considerably smaller than observed at higher temperatures, indicating a tail of relatively mobile Cu ions which may be of significance for potential device applications.

Keywords: Nuclear Magnetic Resonance, thermoelectric materials, superionic conductor, topological electronic behavior

1. Introduction

$Cu_{2-x}Te$ has been of interest as a promising candidate in thermoelectric [1–4] and solar cell [5, 6] applications, and even for cancer treatment [7]. Moreover, it was recently shown to have characteristics associated with topologically nontrivial band inversion [8] and that if formed as a 2D crystal it may exhibit topological insulator characteristics [9]. Topological insulator behavior is also well established [10–13] in Ag_2Se and Ag_2Te. However the $Cu_{2-x}Te$ phase diagram includes structures not fully determined in all cases, and there are several phase transitions at high temperatures [14, 15] as the Te lattice adapts to superionic motion of the Cu ions [16]. The ionic mobility can also induce detrimental effects for device applications. Thus it is important to better understand the structures and their relation to the lattice dynamics and electronic behavior.

$Cu_{2-x}Te$ tends to form spontaneously having nonzero x, and the reported structures are dependent on the Cu vacancy density. Initially, Nowotny [17] reported a hexagonal structure in space group $P6/mmm$ with lattice parameters $a_0 = 4.237$ Å, $c_0 = 7.274$ Å, and $Z = 2$. This structure consists of interconnected Cu-Te layers arranged as 2-dimensional sheets, as shown as an inset in Fig. 1. Later, stoichiometric Cu_2Te was indicated to have a larger superstructure based on the hexagonal structure [18] or an orthorhombic phase [15]. It has also been reported that the structure is trigonal [19, 20] with space group $P\bar{3}m1$, and a recent report [21] predicted that the $P\bar{3}m1$ trigonal phase is stable extending well into the range $x \neq 0$. The phase region $0 \leq x \leq 0.1$ was also described to consist at room temperature of two phases: hexagonal and orthorhombic [14], while recently it was predicted from simulations that Cu_2Te crystallizes in a monoclinic [6] structure with 4 formula units per cell.

Baranova [22–25] reported several specific structures vs. vacancy concentration: β-I (trigonal with space group $P3m1$, a fully-occupied phase with stoichiometry $Cu_7Te_4 = Cu_{1.75}Te$), β-II (hexagonal, space group $P\bar{6}m2$, having partial occupancy also giving composition $Cu_{1.75}Te$), and β-III (trigonal,

*Corresponding author. Tel: +1-979-845-7823
Email address: alisirusi@tamu.edu (Ali A. Sirusi)

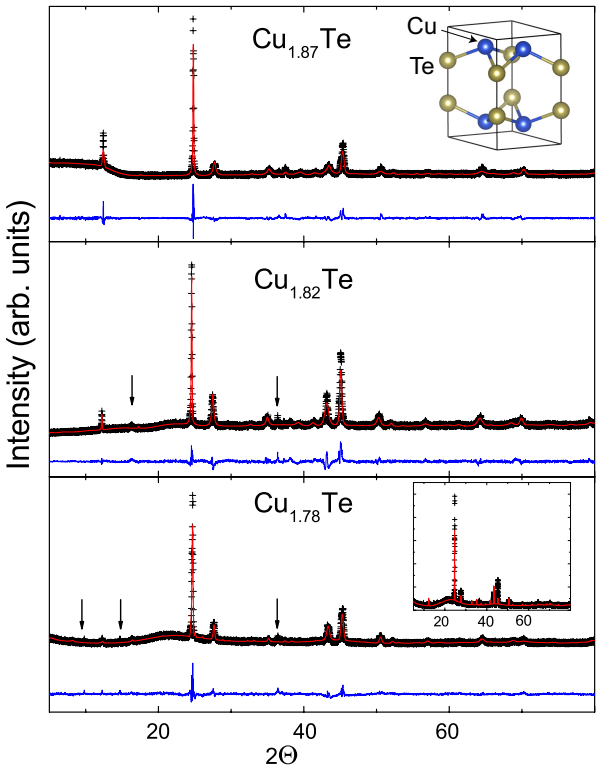

Figure 1: XRD patterns of $Cu_{1.87}Te$, $Cu_{1.82}Te$, and $Cu_{1.78}Te$ samples, with fittings to $P\bar{3}m1$ trigonal structure (first two samples) and β-II structure (for $Cu_{1.78}Te$). Lower inset: $Cu_{1.78}Te$ with fitting to β-I structure. Red lines are fitted curves and blue lines show the differences. Arrows are extra peaks noted in the text. Upper inset: Nowotny structure; fitted structures are larger superstructures with similar layered structure.

space group $P3m1$, partial occupancy corresponding to $Cu_{1.812}Te$). These structures have 6, 7, and 24 distinct Cu sites and 4, 3 and 12 Te sites per cell, for β-I, β-II, and β-III respectively, while the previously mentioned $P\bar{3}m1$ trigonal phase has 4 Cu and 2 Te sites/cell. These structures have closely related lattice parameters, and may be considered to be superstructures of Nowotny's hexagonal structure, with all containing interconnected Cu-Te atomic layers, although the nearest neighbors within the layers and site symmetries differ considerably.

In this report we describe Cu and Te NMR measurements on three $Cu_{2-x}Te$ samples of varying composition from $x = 0.13$ to 0.22, supported by Hall coefficient and structural characterization, and all-electron computation. The samples are in the composition range of this material previously identified as having topologically nontrivial band inversion [8]. A structure change in the range $x = 0.20$ induces a large change in NMR spectra, and we find that the charge carriers can be accounted for in a relatively straightforward way, as a heavily doped semiconductor with holes contributed by Cu vacancies. Furthermore the barriers for low-temperature Cu hopping become progressively smaller as the vacancy density increases, with a very small barrier obtained for $x = 0.22$.

2. Experimental and Computational methods

2.1. Synthesis and Experimental Methods

Sample ingots were made by melting followed by annealing. First, Cu shot (Alfa Aesar 99.9999%) and Te pieces (Alfa Aesar 99.9999%) totaling 15 grams were sealed in vacuum in a graphite coated quartz tube, with a mole ratio corresponding to Cu_2Te. The tube was heated over a period of seven hours to 1393 K, then held there for three hours and naturally cooled to room temperature. The resulting ingot was polished and then powderized in an agate mortar and pestle. The powder was divided into three parts and cold pressed into pellets, which were placed in separate evacuated quartz tubes and annealed at 750 K, 850 K, and 1000 K for one week. In each case, a heating rate of 50 C/hr and a cooling rate of 25 C/hr was used for annealing. The ingots from this process were then polished and cut into bars for further measurements.

In backscattered electron images collected using a Cameca SXFive Electron Probe Micro-Analyzer,

contrast indicated phase uniformity, with no secondary phases detected. This was followed by wavelength dispersion spectroscopy (WDS) measurements on at least four points on each sample, with compositions from each point showing variations of 0.3 at.% or less. From the mean values, the WDS results showed the samples annealed at 750, 850, and 1000 K to have compositions $Cu_{1.78}Te$, $Cu_{1.82}Te$, and $Cu_{1.87}Te$ respectively. The samples are denoted below according to these compositions.

As noted above, $Cu_{2-x}Te$ tends to form spontaneously with a Cu deficit ($x > 0$), and apparently this occurs during the initial formation of the ingot from the melt. The different compositions after the anneal processes can be understood to occur due to preferential evaporation of Te due to its larger vapor pressure.

Structural characterization via powder x-ray diffraction (XRD) was performed on a Bruker D8 X-ray Powder Diffractometer with Cu Kα radiation. To analyze the results Rietveld refinements were performed using EXPGUI software [26, 27]. The Hall coefficient was measured at ambient temperature using an AC 4-probe method in a custom built apparatus under a maximum field of 1 Tesla, and also at low temperatures using a Quantum Design, Inc. MPMS combined with a home-built bridge

The NMR techniques were similar to those described elsewhere [8], with echo integration used to obtain static line shapes in a fixed 9 T field. Solid CuCl and aqueous $Te(OH)_6$ standards were used for Cu and Te references with positive relative shifts having paramagnetic sign (δ convention). $Te(OH)_6$ has a shift of +707 ppm relative to the primary standard [28], $(CH_3)_2Te$, and the spectra have been adjusted accordingly. ^{63}Cu NMR spectra were fitted using the DmFit package [29]. The chemical shift (δ_{cs}) and Knight shift (K) were defined relative to the total shift (δ) according to $\delta = \delta_{cs} + K$, with K identified according to metallic shift theory, as representing the electron spin contribution in absence of spin-orbit coupling.

NMR spin-lattice relaxation (T_1) measurements used an inversion-recovery sequence, with T_1 as fitting parameter within a multi-exponential magnetic relaxation function $[M(t_{wait})/M(0) = 1 - \alpha(0.1e^{-t_{wait}/T_1} + 0.9e^{-6t_{wait}/T_1})]$, as previously reported [8] for the ^{63}Cu and ^{65}Cu central transitions. At 77 K a small quadrupole contribution to $1/T_1$ was isolated by setting $1/T_1$ equal to a sum of two contributions [30] and using standard values [8] for the nuclear magnetic and quadrupole moments. For ^{125}Te, which has spin 1/2, we used the function $[M(t_{wait})/M(0) = 1 - \alpha e^{-t_{wait}/T_1}]$.

2.2. Computational Methods

Density functional theory (DFT) calculations were carried out using the WIEN2k code [31, 32] to determine electric field gradients (EFGs) and model the Cu NMR spectra, and for energy minimization of the structures. These were performed with the Generalized Gradient Approximation (GGA) using the PBE exchange potential [33], with 200 k-points, and $Rk_{max} = 7$. Calculations done on reported Cu_2Te structures used experimental lattice constants from the literature, but with internal parameters minimized. Although in some cases partial occupation of Cu sites was given in reported structures, for DFT computations we set occupation numbers equal to 1 (compositions Cu_2Te except for β-I, which is Cu_7Te_4 with all sites filled).

3. Results and Analysis

3.1. Structure and Transport Results

XRD patterns are shown in Fig. 1. A prominent feature is that with lower annealing temperature and increased vacancy density the peak intensity at $2\Theta = 12.3°$ is reduced. This is accompanied by appearance of several small additional peaks as shown in the figure (arrows). The XRD patterns for $Cu_{1.87}Te$ and $Cu_{1.82}Te$ have similar features and were fitted using the $P\bar{3}m1$ trigonal structure [19–21], while the $Cu_{1.78}Te$ result was fitted using the β-II hexagonal structure [24]. For $Cu_{1.87}Te$ and $Cu_{1.82}Te$, internal structural parameters were taken from Ref. [21] with site occupations set to 100%, since the powder fits were found not very sensitive to the partial occupancy of Cu sites as reported. Refinements of the unit cell (trigonal space group $P\bar{3}m1$, #164) yielded lattice parameters $a = 8.362$ and $c = 7.219$ Å for $Cu_{1.87}Te$, and $a = 8.365$ and $c = 7.226$ Å for $Cu_{1.82}Te$, similar to the reported [19–21] $a = 8.37$ and $c = 7.16$ Å for this structure. Fitted cell volumes are 109.3 and 109.5 Å^3, respectively when reduced by 1/4 corresponding to the underlying $Z = 2$ Nowotny hexagonal cell. However note that the β-III structure of Baranova worked equally well (not shown) in fitting the XRD patterns for these two samples, with suitable adjustment of the reported [22] lattice parameters $a = 8.37$ and $c = 21.60$ Å, representing in

this case a larger superstructure with the trigonal space group $P3m1$ (#156). Thus as has been noted previously with powder XRD alone it is difficult to distinguish these structures.

$Cu_{1.78}Te$ refinement yielded $a = 4.161$ and $c = 21.60$ Å in the $P\bar{6}m2$ (#187) β-II structure, also with all Cu sites set to 100% filled. This is comparable to the reported [24] $a = 4.17$ and $c = 21.65$ Å. The refined values yield a reduced cell volume of 107.9 Å^3 when multiplied by 1/3 based on the c-direction supercell. Compared to the other two samples the lattice parameters and cell volume are thus significantly smaller, reflecting the change in structure going to $x = 0.22$. Changes in NMR spectra described below further demonstrate the differing structures for these compositions, a result at variance with the computation-based result [21] that the $P\bar{3}m1$ trigonal structure has the lower energy for the entire composition range. We found that the alternative β-I, Cu_7Te_4 structure proposed for this region of the phase diagram [23] could also be indexed to the XRD pattern, but with some intensity differences involving the reflections near 41 and 42° (inset, Fig. 1).

Hall measurements indicated all $Cu_{2-x}Te$ samples to be heavily-doped p-type, with hole concentrations scaling with Cu vacancy concentration x. Results at ambient temperature correspond to hole concentrations $p = 6.5 \times 10^{21}$, 4.1×10^{21}, and 3.6×10^{21} cm^{-3} for $Cu_{1.78}Te$, $Cu_{1.82}Te$, and $Cu_{1.87}Te$, respectively. For $Cu_{1.82}Te$ and $Cu_{1.87}Te$ measurements were also performed down to liquid helium temperatures, with results showing a variation in p of about 10% vs. temperature, with a weak plateau near 100 K in a manner very similar to what was reported previously in this phase range [3].

Estimated carrier concentrations, assuming one hole per Cu vacancy, can be obtained using the fitted XRD cell volumes. This leads to $p = 4.1 \times 10^{21}$, 3.3×10^{21}, and 2.4×10^{21} cm^{-3} for the $Cu_{1.78}Te$, $Cu_{1.82}Te$, and $Cu_{1.87}Te$ samples, respectively. The Hall results thus scale with composition, pointing to the filling of hole pockets starting with the parent composition Cu_2Te as a semiconductor. There has been uncertainty about this, with calculated electronic properties generally reporting to give metallic or semimetallic behavior [34, 35]. The latter may be due to density functional methods which underestimate the gap [8] and/or uncertainty in the correct structure. The results also point to carriers numbering more than one per vacancy, which may be related to partial covalency of Cu-Te bonding, a result also previously indicated by calculations for the Cu_2Te Nowotny structure [34]. Removing Cu can in this case leave dangling bonds which may remove more than one electron from the valence band.

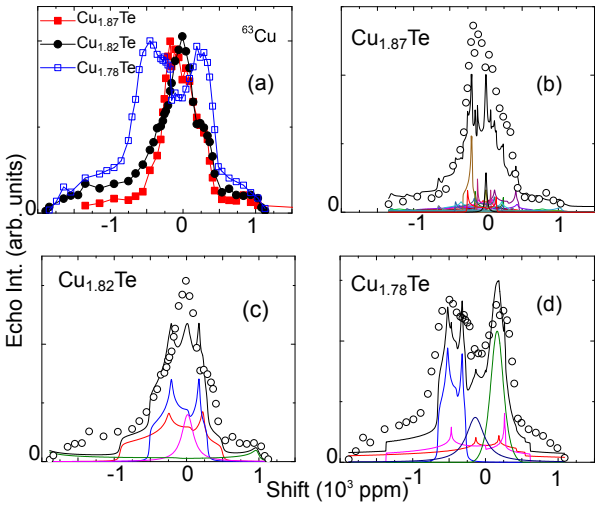

Figure 2: (a) ^{63}Cu spectra of different samples measured at 290 K. (b)-(d): individual spectra along with DFT-calculated line shapes described in the text, for: (b) β-III structure of Baranova [22], (c) $P\bar{3}m1$ trigonal structure, and (d) $P3m1$ β-I structure [24].

3.2. Cu NMR Results

^{63}Cu NMR spectra obtained at 290 K are shown in Fig. 2(a). Each spectrum consists of superposed quadrupole-broadened central transitions (1/2 to −1/2) for each site. The $Cu_{1.87}Te$ and $Cu_{1.82}Te$ results are similar to those reported recently for a similar composition [8], however the $Cu_{1.78}Te$ spectrum exhibits a distinctive splitting with two main peaks, corresponding to its different structure as outlined above.

^{63}Cu spin-lattice relaxation times (T_1) vs. temperature are shown in Fig. 3, measured at the peak amplitude positions for $Cu_{1.87}Te$ and $Cu_{1.82}Te$, and at a position between the two prominent peaks for $Cu_{1.78}Te$. ^{65}Cu T_1 measurements were also performed at fixed temperatures of 4.2 K, 77 K, and 290 K, allowing the relative contributions due to electric quadrupole vs. magnetic mechanisms to be assessed. For all three samples it was found that a magnetic mechanism strongly dominates at 77 K, with the ratios $^{63}T_1/^{65}T_1$ equal to 1.13, 1.12, and 1.14 respectively for $Cu_{1.87}Te$, $Cu_{1.82}Te$, and $Cu_{1.78}Te$, compared the the expected ratio [8]

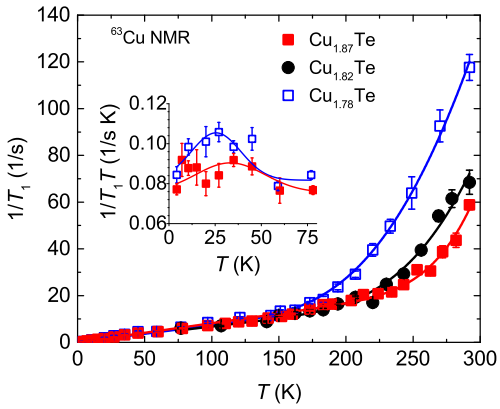

Figure 3: ^{63}Cu $1/T_1$ vs temperature for the three samples as indicated. Solid curves are fits as explained in the text. Inset: $1/T_1T$ vs. T for $Cu_{1.87}Te$ and $Cu_{1.78}Te$ at low temperatures with curves: guides to the eye.

$^{65}\gamma^2/^{63}\gamma^2 = 1.14$, vs. $^{65}Q^2/^{63}Q^2 = 0.85$ for a pure quadrupole relaxation mechanism. Thus we analyzed the 77 K results according to a Korringa mechanism due to metallic carriers [36]. On the other hand the ratios indicate that a quadrupole mechanism becomes dominant at 290 K as ionic hopping becomes enhanced, in good agreement with previously reported results [8]. Futhermore there is a small departure from $1/T_1T$ = constant behavior below about 50 K for $Cu_{1.78}Te$ (inset, Fig. 3), and the ^{63}Cu/^{65}Cu ratios at 4 K also indicate reappearance of a quadrupole contribution, signaling perhaps an effect of local vibrational modes with strong anharmonicity [37]. As shown in the inset, the effect becomes small or absent for the $Cu_{1.87}Te$ sample. There has been previous interest in low-energy modes exhibited by other superionic conductors [38].

Analyzing for ionic motion approaching room temperature, $1/T_1$ could be fitted over the full range [8] to $f\exp(-\Delta E/k_BT) + BT$, where ΔE is the activation energy and BT represents primarily the metallic contribution. Least squares fitting (solid curves in Fig. 3) gave $\Delta E = 0.21$, 0.16, and 0.12 eV for $Cu_{1.87}Te$, $Cu_{1.82}Te$, and $Cu_{1.78}Te$, respectively, with ΔE thus becoming strongly reduced with increasing vacancy density, and with the change in superstructure going to $Cu_{1.78}Te$. These activation energies are smaller than have been reported from higher-temperature measurements [39, 40], indicating a population of ions that is particularly mobile at low T. Also the results are consistently smaller than found in the previous NMR measurement [8], the latter involving a sample formed by spark plasma sintering, indicating perhaps that grain refinement by spark plasma sintering helps to immobilize Cu ions. The $Cu_{1.78}Te$ sample with lowest barrier also exhibited the peak in low temperature $1/T_1T$, and thus the small Cu-ion hopping barriers in this sample may also be connected to the presence of low energy localized vibrational modes.

Regarding the magnetic contribution (T_{1M}) dominant at 77 K, note that for the measured carrier densities, assuming parabolic hole pockets, as previously shown [8] the doping is well into the metallic regime. Thus Korringa behavior ($K^2T_{1M}T$ = constant) will apply, with K = Knight shift. For the simple metallic case, or as long as correlation effects remain independent of p [36, 41], $1/T_{1M}T \propto g^2(E_F)$, and $g(E_F) \propto \sqrt{E_F} \propto p^{1/3}$, where $g(E_F)$ is the Fermi-level electronic density of states and p is the hole density. Therefore $1/T_{1M}$ vs. $p^{2/3}$ should be linearly related. Fig. 4 shows such a plot, with $1/T_{1Q}$ contributions (10% or less relative to $1/T_{1M}$) subtracted as described above. Carrier densities plotted are the measured values for 77 K, except for $Cu_{1.78}Te$. The previously reported value [8] has been included in the plot as an open circle, and it is seen that the results fall in line as expected, including the $Cu_{1.78}Te$ result for which the superstructure has changed. Together with the Hall results this indicates carriers filling a single parabolic hole pocket with no compensation. As noted above, DFT calculations [42] in the Nowotny structure have indicated the material to be metallic with multiple band crossings, but these results are likely affected by DFT methods underestimating the gap and/or uncertainty in crystal structure.

Fitting the central regions of the $Cu_{1.87}Te$ and $Cu_{1.82}Te$ ^{63}Cu spectra with Gaussian curves yields an approximate measure of their shift positions, -50 ppm and -24 ppm respectively, making an assumption as before [8] that the sharp peak is contributed mainly by a site with small spectral width. Using measured $1/T_1$ values as described above, and assuming $K^2T_1T = 3.7 \times 10^{-6}$ sK, for ^{63}Cu in the simple metallic limit, we obtain K = 520 and 490 ppm, and hence $\delta_{cs} = -570$ and -510 ppm, respectively, close to the estimated $\delta_{cs} = -490$ ppm peak position of the previous sample [8]. A similar analysis for $Cu_{1.78}Te$ yields K = 600 and 570 ppm for the two peaks, an indication that the much larger splitting observed for this composition

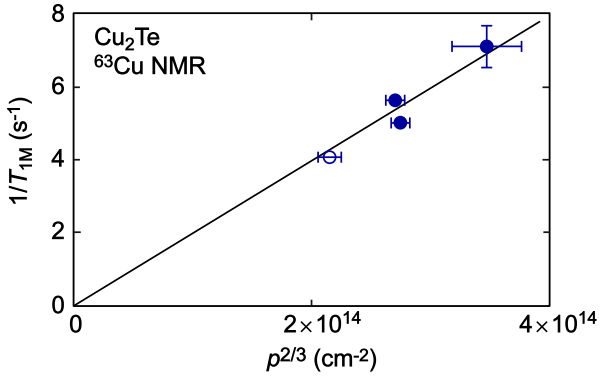

Figure 4: ^{63}Cu $1/T_{1M}$ for $T = 77$ K, plotted vs $p^{2/3}$, where p is the measured hole density. Open circle: previously reported value [8]. Straight line is least-squares fitted line through zero. Vertical error bars for $Cu_{1.78}Te$ sample encompasses range of measured values, including measurements at two peaks in spectrum and at line shape center.

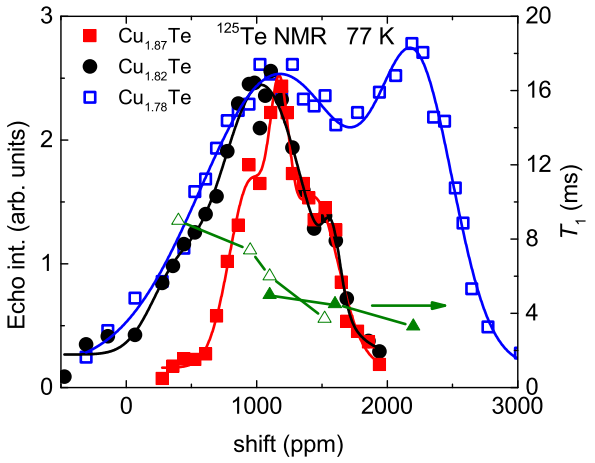

Figure 5: ^{125}Te spectra for 3 samples measured at 77 K. Solid curves from a fitted sum of 2 or 3 Gaussian curves intended to guide the eye. Also shown: T_1 measured at selected positions for $Cu_{1.82}Te$ (open triangles) and $Cu_{1.78}Te$ (solid triangles), plotted against right axis.

is due instead to differences in chemical shift and/or quadrupole contributions.

3.3. Te NMR Results

Fig. 5 shows ^{125}Te spectra at 77 K. The line shape and overall shift for $Cu_{1.87}Te$ is essentially identical to the previous result [8] for a composition with slightly smaller carrier density. The $Cu_{1.82}Te$ result is somewhat broader a more negative shift, while the $Cu_{1.78}Te$ line shape is very different corresponding to its modified crystal structure, and in line with the Cu NMR results described above.

^{125}Te has spin 1/2 and does not experience electric quadrupole broadening, in contrast to the Cu nuclei, and as a result the $^{125}T_1$ is magnetic-only, dominated in this case by charge carriers. As shown in Fig. 5 for $Cu_{1.82}Te$ and $Cu_{1.78}Te$, T_1 decreases with increasing shift when sampled across the line shapes. This indicates that a distribution of Knight shifts is a main feature determining the line shapes; similar results were obtained for $Cu_{1.87}Te$.

Regarding the Te Knight shifts, assuming $K = 0$ at $\delta_{cs} = -1170$ ppm, the mean value identified previously [8], with T_1 measured at line-center positions we obtain $K^2T_1T = 2.7$, 2.5, and 3.2 $\times 10^{-6}$ sK for $Cu_{1.78}Te$, $Cu_{1.82}Te$, and $Cu_{1.87}Te$, respectively, compared to 2.6 $\times 10^{-6}$ sK for simple metallic behavior [36, 41]. The results help to confirm the assumption of Korringa behavior with small or zero enhancement. Note however that the decrease in T_1 sampled across the split $Cu_{1.78}Te$ line is not as large as expected for purely Korringa behavior. For example assuming $K^2T_1T = 2.6 \times 10^{-6}$ sK across the line, T_1 for the left and right peaks (Fig. 5) gives $K = 2600$ and 3200 ppm respectively, and correspondingly $\delta_{cs} = -1500$ and -1000, thus perhaps a 500 ppm chemical shift contribution to the observed splitting. Similarly for $Cu_{1.87}Te$ assuming an unenhanced $K^2T_1T = 2.6 \times 10^{-6}$ sK gives a renormalized $\delta_{cs} = -1000$ ppm, a small difference perhaps mainly responsible for its observed difference in peak position relative to $Cu_{1.82}Te$. Since K contributions are large, these differences fall within the uncertainty of the analysis [8], however the large negative δ_{cs}, along with Korringa behavior indicating a significant s-symmetry contribution to the valence band edge, are consistent with and reinforce the previous results giving evidence for topologically nontrivial behavior [8]. These shifts can be compared to observed ^{125}Te shifts for molecular systems falling in the range of about $\delta = -800$ to +2300 ppm [43, 44], while recent reports in semiconductors for which K contributions were believed small include ZnTe [45], −875 ppm, and the inverted-band [46] PbTe (−1150 ppm) and SnTe (−970 ppm), along with GeTe (−230 ppm), with all values renormalized according to shift reagent.

3.4. Computational Results

DFT calculations in the four structures discussed above (β-I, β-II, β-III, and $P\bar{3}m1$ trigonal) were used to calculate electric field gradients (EFGs), and thus the Cu quadrupole NMR lineshapes. These methods have been shown to work

well in computing quadrupole NMR parameters, often within 10–20% of experimental values and thus providing a means to examine local structures [32]. Fig. 2(b-d) shows some of the results. Part (b) of the figure shows the model curve obtained from the β-III structure calculation plotted with the $Cu_{1.87}Te$ ^{63}Cu NMR data. The low-intensity curves in the figure are individual lines for each of the 24 Cu sites, while the upper curve is the summed line shape. A single overall scaling parameter was applied to match the amplitude to the experimental data. As noted above, the DFT calculations were performed for full site occupancy rather than with random vacancies included, and the major effect of localized vacancies on the NMR spectra will be a broadening process. The absence of the sharp peaks in the experimental spectra, as compared to the computed curves, is thus likely due to the distribution of vacancies in the samples. The match for the data in Fig. 2(b) is thus reasonable, including the wings extending to large positive and negative shifts which arise from sites having relatively large EFG tensors with nonzero asymmetry.

The calculation for the $P\bar{3}m1$ trigonal structure is shown in Fig. 2(c), plotted with the $Cu_{1.82}Te$ results. This structure has only 4 inequivalent Cu sites. The generally smaller EFG's resulting from this structure lead to a smaller line width, and it appears that this structure does not fit the NMR results for either $Cu_{1.87}Te$ or $Cu_{1.82}Te$. Also, while this method of computing EFG's is not relevant for the Te NMR results, the $P\bar{3}m1$ trigonal structure with only two Te sites also does not agree with the Te NMR results, since the variation of T_1 across the line and the structure of the NMR spectra are indicative of a superposition of three or more distinct sites. Thus the β-III structure provides the better match for these two compositions.

The two structures β-I and β-II provided the best agreement of XRD results to the $Cu_{1.78}Te$ composition. Among these, in the computed β-II results all Cu sites have axial symmetry, hence an EFG tensor with relatively constrained second-order quadrupole line shapes. The resulting Cu NMR spectrum has no intensity outside the range -750 to $+250$ ppm, and thus provides a poor fit to the data. Note that anisotropic chemical and Knight shift contributions are not included in the calculated results, but these are expected to be considerably smaller that the observed width. On the other hand the calculation based on the β-I structure provided a reasonable match, as shown in Fig. 2(d). In modeling the results, different sites provide the main source of intensity for the two main observed peaks in the spectrum, a result which is reasonable given the different observed T_1 results for these positions.

4. Conclusion

We performed ^{63}Cu, ^{65}Cu, and ^{125}Te NMR on $Cu_{2-x}Te$ with x between 0.13 and 0.22, along with transport and structural measurements. The results agree with the phase diagram proposed by Baranova, with a phase change near $x = 0.20$ fitted to a transition from the β-III structure for $x =$ 0.13–0.18 to β-I for larger x. These compositions have been variously described as metallic or semiconducting, however the Hall and Korringa NMR behavior are shown here to correspond to filling of simple uncompensated hole pockets, behavior which extends across the phase boundary. The Korringa analysis also allows identification of the Cu and Te NMR chemical shifts, shown to fall at the far negative end of the expected shift ranges for all compositions. This behavior was previously identified with topologically nontrivial inverted band configuration. For the $x = 0.22$ structure there is a large splitting in chemical shift corresponding to two rather different local environments for both Cu and Te sites. Furthermore the activation energy for initiation of Cu ion hopping near room temperature is rapidly reduced with increased Cu vacancies to 0.12 eV for $x = 0.22$. These barriers are considerably smaller than detected at higher temperatures, indicating a tail of relatively mobile ions which may have important consequences for device applications.

Acknowledgement

This work was supported by the Robert A. Welch Foundation, Grant No. A-1526, and also by the Department of Energy, with support under the Office of Basic Energy Sciences Award # DE-SC-0008574.

References

[1] K. Sridhar, K. Chattopadhyay, Synthesis by mechanical alloying and thermoelectric properties of Cu_2Te, J. Alloys Compd. 264 (1998) 293 – 298.

[2] H. Liu, X. Shi, F. Xu, L. Zhang, W. Zhang, L. Chen, Q. Li, C. Uher, T. Day, G. J. Snyder, Copper ion liquid-like thermoelectrics, Nature Mater. 11 (2012) 422.

[3] S. Ballikaya, H. Chi, J. R. Salvador, C. Uher, Thermoelectric properties of Ag-doped Cu_2Se and Cu_2Te, J. Mater. Chem. A 1 (2013) 12478.

[4] Y. He, T. Zhang, X. Shi, S.-H. Wei, L. Chen, High thermoelectric performance in copper telluride, NPG Asia Mater. 7 (2015) e210.

[5] J. H. Yun, K. H. Kim, D. Y. Lee, B. T. Ahn, Back contact formation using Cu_2Te as a Cu-doping source and as an electrode in CdTe solar cells, Solar Energy Mater. Solar Cells 75 (2003) 203 – 210.

[6] M. C. Nguyen, J.-H. Choi, X. Zhao, C.-Z. Wang, Z. Zhang, K.-M. Ho, New layered structures of cuprous chalcogenides as thin film solar cell materials: Cu_2Te and Cu_2Se, Phys. Rev. Lett. 111 (2013) 165502.

[7] A. C. Poulose, S. Veeranarayanan, M. S. Mohamed, R. R. Aburto, T. Mitcham, R. R. Bouchard, P. M. Ajayan, Y. Sakamoto, T. Maekawa, D. S. Kumar, Multifunctional $Cu_{2-x}Te$ nanocubes mediated combination therapy for multi-drug resistant MDA MB 453, Sci. Rep. 6 (2016) 35961.

[8] A. A. Sirusi, S. Ballikaya, J.-H. Chen, C. Uher, J. H. Ross, Band ordering and dynamics of $Cu_{2-x}Te$ and $Cu_{1.98}Ag_{0.2}Te$, J. Phys. Chem. C 120 (27) (2016) 14549–14555.

[9] Y. Ma, L. Kou, Y. Dai, T. Heine, Two-dimensional topological insulators in group-11 chalcogenide compounds: $M_2Te(M = Cu, Ag)$, Phys. Rev. B 93 (2016) 235451.

[10] W. Zhang, R. Yu, W. Feng, Y. Yao, H. Weng, X. Dai, Z. Fang, Topological aspect and quantum magnetoresistance of $\beta - Ag_2Te$, Phys. Rev. Lett. 106 (2011) 156808.

[11] S. Lee, J. In, Y. Yoo, Y. Jo, Y. C. Park, H. jun Kim, H. C. Koo, J. Kim, B. Kim, K. L. Wang, Single crystalline β-Ag_2Te nanowire as a new topological insulator, Nano Lett. 12 (2012) 4194–4199.

[12] A. Sulaev, W. Zhu, K. L. Teo, L. Wang, Gate-tuned quantum oscillations of topological surface states in $\beta - Ag_2Te$, Sci. Rep. 5 (2015) 8062.

[13] J. Kim, A. Hwang, S.-H. Lee, S.-H. Jhi, S. Lee, Y. C. Park, S.-i. Kim, H.-S. Kim, Y.-J. Doh, J. Kim, B. Kim, Quantum electronic transport of topological surface states in $\beta - Ag_2Se$ nanowire, ACS Nano 10 (2016) 3936–3943.

[14] Y. G. Asadov, L. V. Rustamova, G. B. Gasimov, K. M. Jafarov, A. G. Babajev, Structural phase transitions in $Cu_{2-x}Te$ crystals ($x = 0.00, 0.10, 0.15, 0.20, 0.25$), Phase Transit. 38 (1992) 247–259.

[15] R. Blachnik, M. Lasocka, U. Walbrecht, The system copper-tellurium, J. Solid State Chem. 48 (1983) 431 – 438.

[16] J. Boyce, B. Huberman, Superionic conductors: Transitions, structures, dynamics, Phys. Rep. 51 (1979) 189–265.

[17] H. Nowotny, Die kristallstructur von Cu_2Te, Z. Metallkd. 37 (1946) 40.

[18] I. Patzak, Uber die struktur und die lage der phasen im system kupfer-tellur, Z. Metallkd. 47 (1956) 418.

[19] S. Matar, R. Weihrich, D. Kurowski, A. Pfitzner, DFT calculations on the electronic structure of $CuTe_2$ and Cu_7Te_4, Solid State Sci. 6 (2004) 15–20.

[20] D. P. D. Kurowski, Ph.D. thesis, University of Regensburg, Germany (2003).

[21] L. Yu, K. Luo, S. Chen, C.-G. Duan, Cu-deficiency induced structural transition of $Cu_{2-x}Te$, CrystEngComm 17 (14) (2015) 2878–2885.

[22] R. V. Baranova, A. S. Avilov, Z. G. Pinsker, Determination of crystal-structure of hexagonal phase β-III in Cu-Te system by electron-diffraction method, Kristallografiya 18 (1973) 1169.

[23] R. V. Baranova, Electron diffraction determination of the structure of the β-I phase in the Cu-Te system, Kristallografiya 12 (1967) 266.

[24] R. V. Baranova, Electron diffraction determination of the crystal structure of the hexagonal phase β-II in the Cu-Te system, Kristallografiya 13 (1968) 803.

[25] R. V. Baranova, Crystal structure determination by electron diffraction of the hexagonal β double phase in the Cu-Te system, Sov. Phys. Crystallogr. 13 (1969) 695–699.

[26] B. H. Toby, *EXPGUI*, a graphical user interface for *GSAS*, J. Appl. Crystallogr. 34 (2001) 210–213.

[27] A. C. Larson, R. B. V. Dreele, Los Alamos National Laboratory Report LAUR (1994) 86–748.

[28] M. Inamo, ^{125}Te NMR evidence for the existence of trinuclear tellurate ion in aqueous solution, Chem. Lett. 25 (1996) 17–18.

[29] D. Massiot, F. Fayon, M. Capron, I. King, S. Le Calvé, B. Alonso, J.-O. Durand, B. Bujoli, Z. Gan, G. Hoatson, Modelling one- and two-dimensional solid-state NMR spectra, Magn. Reson. Chem. 40 (2002) 70–76.

[30] A. A. Sirusi, J. H. Ross, Pseudogap and anharmonic phonon behavior in $Ba_8Ga_{16}Ge_{30}$: An NMR study, J. Chem. Phys. 145 (2016) 054702.

[31] P. Blaha, K. Schwarz, G. Madsen, D. Kvasnicka, J. Luitz, WIEN2k, an Augmented Plane Wave+Local Orbitals Program for Calculating Crystal Properties, Technische Universität Wien, Austria, 2001.

[32] K. Schwarz, P. Blaha, Solid state calculations using WIEN2k, Comput. Mater. Sci. 28 (2003) 259–273.

[33] J. P. Perdew, K. Burke, M. Ernzerhof, Generalized gradient approximation made simple, Phys. Rev. Lett. 77 (1996) 3865–3868.

[34] S. Kashida, W. Shimosaka, M. Mori, D. Yoshimura, Valence band photoemission study of the copper chalcogenide compounds, Cu_2S, Cu_2Se and Cu_2Te, J. Phys. Chem. Solids 64 (2003) 2357–2363.

[35] Y. Zhang, Y. Wang, L. Xi, R. Qiu, X. Shi, P. Zhang, W. Zhang, Electronic structure of antifluorite Cu_2X (X = S, Se, Te) within the modified Becke-Johnson potential plus an on-site Coulomb U, J. Chem. Phys. 140 (2014) 074702.

[36] J. Korringa, Nuclear magnetic relaxation and resonance line shift in metals, Physica 16 (1950) 601 – 610.

[37] X. Zheng, S. Y. Rodriguez, J. H. Ross, Jr., NMR relaxation and rattling phonons in the type-I $Ba_8Ga_{16}Sn_{30}$ clathrate, Phys. Rev. B 84 (2011) 024303.

[38] K. Wakamura, Origin of the low-energy mode in superionic conductors, Phys. Rev. B 59 (1999) 3560–3568.

[39] S.-Y. Miyatani, S. Mori, M. Yanagihara, Phase diagram and electrical properties of $Cu_{2-\delta}Te$, J. Phys. Soc. Jpn. 47 (1979) 1152–1158.

[40] R. A. Yakshibaev, N. N. Mukhamadeeva, R. F. Almukhametov, Phase transformations and ionic transport in the $Cu_{2-\delta}Te$ superionic conductor, Phys. Status Solidi (a) 108 (1988) 135–141.

[41] G. C. Carter, L. H. Bennett, D. J. Kahan, Metallic shifts in NMR, Prog. Mater. Sci. 20.

[42] Y. Zhang, B. Sa, J. Zhou, Z. Sun, First principles investigation of the structure and electronic properties of Cu_2Te, Comp. Mater. Sci. 81 (2014) 163–169.

[43] Y. Ruiz-Morales, G. Schreckenbach, T. Ziegler, Calculation of ^{125}Te chemical shifts using gauge-including atomic orbitals and density functional theory, J. Phys. Chem. A 101 (22) (1997) 4121–4127.

[44] H. Günther, NMR Spectroscopy: Basic Principles, Concepts and Applications in Chemistry, Wiley-VCH, Siegen, Germany, 2013.

[45] D. Koumoulis, G. D. Morris, L. He, X. Kou, D. King, D. Wang, M. D. Hossain, K. L. Wang, G. A. Fiete, M. G. Kanatzidis, L.-S. Bouchard, Nanoscale β-nuclear magnetic resonance depth imaging of topological insulators, Proc. Natl. Acad. Sci. USA 112 (28) (2015) E3645–E3650.

[46] B. Njegic, E. Levin, K. Schmidt-Rohr, ^{125}Te NMR chemical-shift trends in PbTe–GeTe and PbTe–SnTe alloys, Solid State Nucl. Mag. Reson. 55-56 (2013) 79–83.